

Ultrasound-Induced Dissolution of Lipid-Coated and Uncoated Gas Bubbles

Debra J. Cox and James L. Thomas*

Department of Physics and Astronomy, University of New Mexico, Albuquerque, New Mexico 87008

Received June 25, 2010. Revised Manuscript Received August 6, 2010

The 1.1 MHz ultrasound response of micrometer-scale perfluorobutane gas bubbles, coated with a mixture of 90 mol % saturated phospholipid (distearylphosphatidylcholine, DSPC) or unsaturated phospholipid (dioleoylphosphatidylcholine, DOPC) and 10 mol % PEG-lipid, was studied by optical microscopy. Uncoated bubbles were also studied. Bubbles, resting buoyantly against the wall of a polystyrene cuvette, were exposed to brief pulses of ultrasound (~200 kPa amplitude) at a repetition rate of 25 Hz; images of the bubbles were taken after every other pulse. The coating had little effect on the initial response: large (> 10 μm diameter) bubbles showed no size change, while smaller bubbles rapidly shrank (or fragmented) to reach a stable or metastable diameter—ca. 2 μm for coated bubbles and 4 μm for uncoated bubbles. The coating had a significant effect on further bubble evolution: after reaching a metastable size, uncoated bubbles and DOPC-coated bubbles continued to shrink slowly and ultimately vanished entirely, while DSPC-coated bubbles did not change perceptibly during the duration of the exposure. Numerical modeling using the modified Herring equation showed that the size range in which DSPC bubbles responded does correspond well with the bubble resonance; the long-term stability of these bubbles may be related to the ability of the DSPC to form a two-dimensional solid at ambient temperature or to phase separate from the PEG-lipid.

1. Introduction

There is considerable interest in the application of high-frequency (megahertz) ultrasound not only to biomedical imaging, but also for therapeutics and targeted delivery of pharmaceuticals. Many different strategies and delivery vehicles have been studied.¹ Ultrasound has been exploited for localized heating, which can be used to dramatically increase liposomal permeability for localized drug delivery.² The cavitating effects of strong ultrasound can be used for tissue disruption; this phenomenon has been explored for enhancing the delivery of drugs across the blood–brain barrier.³ Direct (nonthermal) effects of ultrasound on liposomes, micelles, and lipid-coated bubbles have also been examined. In general, it is not possible to disrupt lipid bilayers (in aqueous suspensions) at sound levels that do not cause spontaneous cavitation and consequent cavitation collapse and shock wave generation, and it will undoubtedly be very difficult to prevent cellular damage under these conditions.⁴ Exogenous gas bubbles, on the other hand, are extremely responsive to even low intensities of ultrasound, owing to the high compressibility of gases compared to water.^{5,6} A number of studies have exploited this fact, with the goal of using the ultrasound-driven volume change and the concomitant surface area change of bubbles to release pharmaceutically active molecules from the bubble surface, principally through the fragmentation and dissolution or dispersion of a surface shell material.³ Phospholipids (or phospholipid/oil mixtures) are commonly used shell materials, in part because such materials are already used in clinical imaging applications; the interested

reader is referred to the review by Unger.⁷ Lipid-based clinical imaging products, such as Definity (Bristol-Myers Squibb), consist predominantly of saturated phospholipids that are solid at body temperature, which is thought to promote bubble stability in circulation.

To further explore the role of the shell or coating on the ultrasound response of micrometer-scale (2–20 μm diameter) gas bubbles, we subjected lipid-coated perfluorobutane bubbles to brief pulses of 1.1 MHz ultrasound. Perfluorobutane is commonly used in such studies, as it has a very low solubility in water. The bubbles were formed using a probe sonicator positioned at the surface of an aqueous suspension of liposomes. These passively coated bubbles had a submonolayer coverage, as determined in separate measurements by quantitative fluorescence microscopy (using a fluorescent dopant). Nonetheless, they showed very different behaviors depending on the phospholipid used as the major constituent (saturated distearylphosphatidylcholine vs unsaturated dioleoylphosphatidylcholine), and both lipid shells showed significant differences compared with unshelled bubbles. Bubbles with the saturated coat lipids ultimately reached a stable size and were resistant to further ultrasonic disruption, as has been observed by others. However, bubbles with the unsaturated coat lipids were completely destroyed on insonation, even though they showed good stability in the absence of ultrasound.

2. Materials and Methods

2.1. Materials. Phospholipids 1,2-distearoyl-*sn*-glycero-3-phosphocholine (DSPC), 1,2-dioleoyl-*sn*-glycero-3-phosphocholine (DOPC), 1,2-distearoyl-*sn*-glycero-3-phosphoethanolamine-*N*-[methoxy(poly(ethylene glycol))-2000] (DSPE-PEG2000), and 1,2-dipalmitoyl-*sn*-glycero-3-phosphoethanolamine-*N*-(7-nitro-2-1,3-benzoxadiazol-4-yl) (NBD-DPPE) in chloroform solution were purchased from Avanti Polar Lipids (Alabaster, AL) and were stored at $-20\text{ }^{\circ}\text{C}$ until use. Perfluorobutane (PFB) was purchased from SynQuest (Alachua, FL). Phosphate buffered saline (PBS) was prepared with 100 mM NaCl and 40 mM Na_2HPO_4 in nanopure water (D13321, Barnstead, Dubuque, IA) and pH adjusted to 7.4 using HCl (measured with a pH meter (UB-10, Denver Instrument, Arvada, CO)).

*Corresponding author. E-mail: jthomas@unm.edu.

(1) Pitt, W. G.; Husseini, G. A.; Staples, B. J. *Expert Opin. Drug Delivery* **2004**, *1*, 37–56.

(2) Ferrara, K. W.; Borden, M. A.; Zhang, H. *Acc. Chem. Res.* **2009**, *42*, 881–892. Needham, D.; Dewhirst, M. *Adv. Drug Deliv. Rev.* **2001**, *53*, 285–305.

(3) Bull, J. L. *Expert Opin. Drug Delivery* **2007**, *4*, 475–493.

(4) Schroeder, A.; Kost, J.; Barenholz, Y. *Chem. Phys. Lipids* **2009**, *162*, 1–16.

(5) Ferrara, K.; Pollard, R.; Borden, M. *Annu. Rev. Biomed. Eng.* **2007**, *9*, 415–447.

(6) Sboros, V. *Adv. Drug Delivery Rev.* **2008**, *60*, 1117–1136.

(7) Unger, E. C.; Porter, T.; Culp, W.; Labell, R.; Matsunaga, T.; Zutshi, R. *Adv. Drug Delivery Rev.* **2004**, *56*, 1291–1314.

2.2. Microbubble Preparation. Microbubbles were formed by entrainment of gas in a lipid suspension, using a probe sonicator, as described elsewhere.⁸ This method is often used in microbubble research.^{9–12} Other methods have recently been developed to produce more monodisperse bubble populations, which provide significant advantages in imaging applications¹³ and may be especially important for safety and regulatory issues in medical applications.¹⁴ These techniques are mainly focused on microfluidic approaches and variations, including electrohydrodynamic atomization (essentially electric-field-assisted droplet formation).^{15–17} However, in this study, we were particularly interested in exploring the fates of individual bubbles, for which a monodisperse population is not required.

Lipid shells consisted of 90 mol % phospholipid (DSPC or DOPC) and 10 mol % DSPE-PEG2000.¹⁸ For fluorescence experiments, 1 mol % NBD-DPPE was substituted for an equimolar amount of phospholipid.¹⁸ Coated microbubbles were prepared by sonication of a multilamellar liposome suspension, prepared as follows: lipid shell components (dissolved in chloroform) were mixed in a glass vial, and chloroform was removed by nitrogen evaporation followed by vacuum desiccation (1 h), leaving a thin, opaque film in the vial. Phospholipids were resuspended in PBS, at a concentration of 5 mg/mL using a vortex mixer (VM-3000, VWR) at room temperature. The vial was then capped with a septum, with a hole for a probe sonicator (VC 130PB, Sonics & Materials, Newton, CT) to go through. The probe sonicator was positioned at the gas–liquid interface, and PFB was flushed into the vial headspace. The phospholipid suspension was sonicated at maximum power (~ 10 W) for 30 s. The microbubbles were allowed to cool slowly under ambient conditions. The lipid solution was reused for up to 1 month (stored in the refrigerator) by re-sonicating at the gas–liquid interface. Microbubbles were used on the same day they were prepared.

Unshelled PFB microbubbles were prepared by sonicating PBS at maximum power for 30 s, with PFB in the vial headspace and the probe sonicator tip positioned at the gas–liquid interface.

2.3. Microbubble Characterization. Bubble suspension was diluted into PBS and examined in the microscope. The microbubble size distributions are shown in Figure 1. The distributions were very broad, but a sufficient number of bubbles of relevant size were easily found.

Epifluorescence microscopy was performed on fluorescent microbubbles using an inverted microscope (Eclipse TE 200, Nikon, Japan), equipped with a CCD (Coolsnap HQ², Photometrics, Tucson, AZ) and a 40 \times objective (Nikon, Japan). Bubbles were separated from fluorescent lipids/liposomes by buoyancy: 3 μ L of freshly prepared fluorescent microbubbles was drawn into a 25 μ L syringe (Hamilton, Reno, NV) which already contained 10 μ L of PBS. Microbubbles were allowed to rise (2 min), and then the bottom 10 μ L was ejected from the syringe. The remaining solution in the syringe was put on a standard microscope slide (VWR) and covered with a coverslip (VWR). Ten images were taken of each field of view (to estimate noise) and adjusted for photobleaching. Images were corrected by dark image subtraction and normalized by the mercury lamp illumination profile.

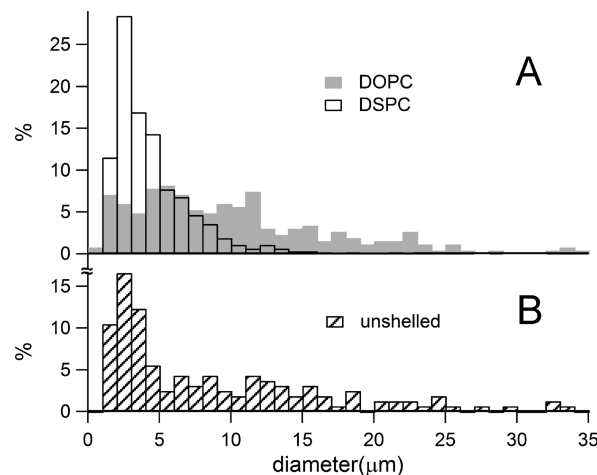


Figure 1. Size distributions for (A) shelled bubbles and (B) unshelled bubbles. 651 DSPC bubbles, 270 DOPC bubbles, and 163 uncoated bubbles were measured. All three were broadly distributed; DOPC was the most broad and more similar to the unshelled than the DSPC distribution.

The brightness per unit surface area of each bubble was determined by integrating all the light from the bubble (using a square region of interest (ROI) with side length $1.316 \times$ bubble diameter, the geometric spread in light for the 0.65 NA objective) and dividing by the surface area of the bubble. The pixel intensities in the ROI were corrected by subtracting background light from out-of-focus bubbles, taken as the average intensity in a 5-pixel “frame” around the ROI.

2.4. Supported Lipid Bilayer Preparation. For calibration of fluorescence intensities, fluorescently doped supported lipid bilayers were used.¹⁹ The lipid bilayers contained 99 mol % DSPC and 1 mol % NBD-DPPE. Phospholipids were suspended in PBS (as above), at a concentration of 1.3 mM. A probe sonicator was positioned near the bottom of the vial, and the lipid solution was sonicated at low power (~ 1 W) for 15 min to form unilamellar liposomes.^{8,20} 35 μ L of liposome solution was pipetted into a Petri dish and covered with a piranha-treated coverslip. This was incubated at a temperature above the lipid main phase transition temperature (55 $^{\circ}$ C for DSPC) for 10 min to allow a supported lipid bilayer to form on the coverglass.

The intensity per unit surface area of the fluorescent bilayer was determined by imaging the bilayer with epifluorescence microscopy, using an inverted microscope (Eclipse TE 200, Nikon, Japan), equipped with a CCD (Coolsnap HQ², Photometrics, Tucson, AZ) and a 40 \times objective (Nikon, Japan).

Image analysis was done with Matlab (MathWorks, Natick, MA). Bilayer images were corrected with a dark image and an illumination profile taken on a uniform fluorescent film. A rectangular area of interest was selected, and the intensity per surface area of the bilayer was calculated as the sum of the pixels in the area of interest, divided by the area (in μm^2) of the area of interest.

2.5. Ultrasound Apparatus. Microbubbles (nonfluorescent) were exposed to short pulses (~ 3 cycles) of ultrasound (US) and imaged after every second pulse. US pulses were generated as follows: square pulses from a function generator (25 Hz) (8012B, Hewlett-Packard, Palo Alto, CA) act as a CCD camera trigger (DFK 31BU03, The Imaging Source, Charlotte, NC) and as the gate input of a programmable function generator (270, Wavetek, San Diego, CA) giving 1.1 MHz 3 μ s (fwhm) Gaussian pulses; the pulses are amplified by a rf power amplifier (ENI 3100LA) to drive a high-intensity focused US transducer (H-101, Sonic Concepts,

(8) Kim, D. H.; Costello, M. J.; Duncan, P. B.; Needham, D. *Langmuir* **2003**, *19*, 8455–8466.

(9) Duncan, P. B.; Needham, D. *Langmuir* **2004**, *20*, 2567–2578.

(10) Feshitan, J. A.; Chen, C. C.; Kwan, J. J.; Borden, M. A. *J. Colloid Interface Sci.* **2009**, *329*, 316–324.

(11) Lozano, M. M.; Longo, M. L. *Langmuir* **2009**, *25*, 3705–3712.

(12) Pu, G.; Borden, M. A.; Longo, M. L. *Langmuir* **2006**, *22*, 2993–2999.

(13) Talu, E.; Hettiarachchi, K.; Powell, R. L.; Lee, A. P.; Dayton, P. A.; Longo, M. L. *Langmuir* **2008**, *24*, 1745–1749.

(14) Stride, E.; Edirisinghe, M. *Soft Matter* **2008**, *4*, 2350–2359.

(15) Farook, U.; Stride, E.; Edirisinghe, M. *J. R. Soc. Interface* **2009**, *6*, 271–277.

(16) Chang, M. W.; Stride, E.; Edirisinghe, M. *Langmuir* **2010**, *26*, 5115–5121.

(17) Pancholi, K.; Stride, E.; Edirisinghe, M. *Langmuir* **2008**, *24*, 4388–4393.

(18) Borden, M. A.; Kruse, D. E.; Caskey, C. F.; Zhao, S. K.; Dayton, P. A.; Ferrara, K. W. *IEEE Trans. Ultrason. Ferroelectr. Freq. Control* **2005**, *52*, 1992–2002.

(19) Werner, J. H.; Montano, G. A.; Garcia, A. L.; Zurek, N. A.; Akhadov, E. A.; Lopez, G. P.; Shreve, A. P. *Langmuir* **2009**, *25*, 2986–2993.

(20) Borden, M. A.; Longo, M. L. *Langmuir* **2002**, *18*, 9225–9233.

Bothell, WA) immersed in a water tank. The pressure amplitude (maximum deviation from ambient) of the pulse at the focus was 400 kPa; the phase of the pulses was 0° (compression before rarefaction).²¹ Pulse characteristics were measured with an HNR 0500 hydrophone (Onda, Sunnyvale, CA).

Microbubble samples ($2 \mu\text{L}$ microbubbles in 5 mL of PBS) were examined in a sealed plastic cuvette positioned at the sonic focus, with its top surface 2 mm below the water surface. Reflection losses from the cuvette wall were accounted for by measuring sound transmission; the hydrophone was positioned behind a partial cuvette (2 cuvette walls were removed, with 2 remaining which were at a right angle to each other). The size of the focus was 1.26 mm, which is larger than the microscope field of view. From these measurements, we estimate the ultrasound pressure amplitude at the bubbles to be $200 \pm 18 \text{ kPa}$ (peak negative pressure = $113 \pm 18 \text{ kPa}$).

A microscope objective (M Plan Apo NIR 20 \times , Mitutoyo, Japan) was used to visualize the microbubbles, transilluminated with a xenon lamp. The microscope objective was focused at the top surface of the cuvette, near the edge of the cuvette closest to the US transducer, to minimize effects of attenuation and scattering by other microbubbles in the path of the US pulse. A sequence of 150 images was taken, with 2 US pulses between each image. Images were analyzed using NIH ImageJ.

3. Results

3.1. Response of Lipid-Coated Microbubbles to Ultrasound. Unshelled microbubbles and microbubbles of two shell compositions (90 mol % DSPC, 10 mol % DSPE-PEG2000 and 90 mol % DOPC, 10 mol % DSPE-PEG2000) were exposed to a sequence of 300 US pulses. A bright-field image was captured every second pulse, for a total of 150 images. The diameter of the microbubble was found for each image in the sequence.

Figure 2 (top) shows typical images of microbubbles taken after the number of ultrasound pulses indicated. Both the DOPC-coated and the uncoated bubble shown vanished before the 200th pulse, while DSPC-coated bubbles persisted throughout the duration of the measurements (300 pulses); these behaviors were found to be typical. Figure 2 (middle) shows a typical plot of the diameters of single microbubbles over a sequence of 300 US pulses. Lipid-coated microbubbles were generally found to shrink to a stable size of $\sim 2 \mu\text{m}$ in diameter: $2.1 \pm 0.8 \mu\text{m}$ (SD) for saturated DSPC and $1.8 \pm 0.7 \mu\text{m}$ for unsaturated DOPC. DSPC-coated bubbles remained at that size for the remainder of the experiment, in agreement with previously published results.^{10,13,18,22,23} In contrast, DOPC-coated bubbles usually disappeared from view in a final, catastrophic shrinkage event. Clearly, the coat on these microbubbles must be shed either before they vanish or during that process itself.

The DOPC-coated microbubbles exhibited three distinct behaviors (Figure 2 (bottom)). Large bubbles ($> 9 \mu\text{m}$ diameter) usually did not respond to ultrasound (one $15 \mu\text{m}$ bubble did shrink, as shown). Smaller bubbles (with one nonresponding exception) either shrank to a metastable size and then disappeared after a delay or dissolved promptly. Only bubbles with diameters $< 4 \mu\text{m}$ showed prompt dissolution, though not all bubbles this small dissolved promptly; many were metastable. Most of the DOPC-coated bubbles eventually dissolved or vanished; only three bubbles (filled symbols) survived the entire duration of observation (300 pulses).

Figure 3 shows the number of surviving small DOPC-coated bubbles as a function of number of US pulses, after bubbles

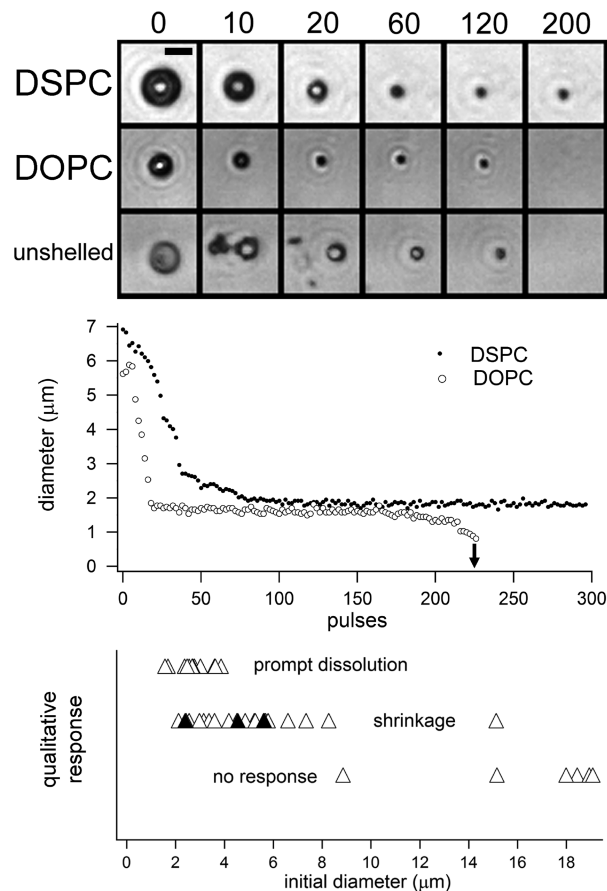


Figure 2. Top: typical images of microbubbles shrinking when exposed to US pulses. The number of pulses is indicated at the top of the figure. Scale bar = $5 \mu\text{m}$. Middle: typical diameter vs pulse number for single microbubbles undergoing dissolution. When exposed to a sequence of ultrasound pulses, 90 mol % DSPC (saturated lipid) microbubbles shrank to a stable diameter of $2.1 \pm 0.8 \mu\text{m}$ and remained at that size for the duration of the experiment. 90 mol % DOPC (unsaturated lipid) microbubbles typically shrank to a slightly smaller metastable diameter, $1.8 \pm 0.7 \mu\text{m}$, but later underwent slight additional shrinkage and then rapidly vanished entirely. Unshelled microbubbles typically fragmented until the core had a diameter of about $4\text{--}6 \mu\text{m}$ and then dissolved away with no stable or metastable size. Bottom: three modes of DOPC-coated microbubble dissolution vs microbubble initial diameter. Large microbubbles did not change size in response to US. Prompt dissolution includes microbubbles that did not reach a stable size and vanished from view in less than 10 pulses. Shrinkage includes microbubbles that shrank to a metastable size. Open triangles are microbubbles that shrank and then vanished within the time frame of the experiment (300 pulses). The three filled triangles represent microbubbles that shrank to a metastable size and survived all 300 pulses.

reached metastable size. The data is well fit by a single exponential with a mean bubble “lifetime” of about 72 pulses, suggesting a fixed probability per pulse for dissolution. However, the actual dissolution event appears *not* to be a single-pulse “catastrophe”, as bubbles show slight but increasing shrinkage just prior to dissolution (as seen at the end of the DOPC trace in Figure 2 (middle)). Thus, the probabilistic event may simply be a precursor to complete dissolution, which is immediately followed by accelerating shrinkage.

The dependence of initial bubble diameter on the US responses of microbubbles is shown in Figure 4, in which the stable (or metastable) bubble diameter is plotted vs the initial bubble diameter, for bubbles coated with saturated (DSPC) or unsaturated (DOPC)

(21) Chomas, J. E.; Dayton, P.; May, D.; Ferrara, K. J. *Biomed. Opt.* **2001**, *6*, 141–150.

(22) Rossi, S.; Waton, G.; Krafft, M. P. *ChemPhysChem* **2008**, *9*, 1982–1985.

(23) Kwan, J. J.; Borden, M. A. *Langmuir* **2010**, *26*, 6542–6548.

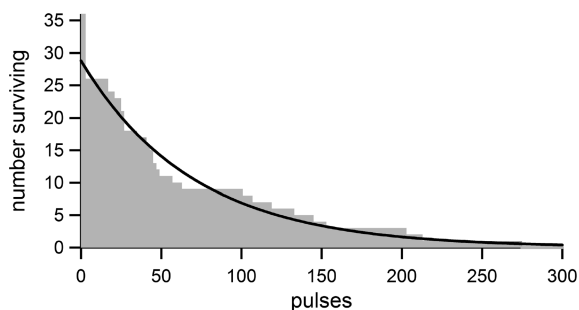


Figure 3. Number of surviving DOPC-coated microbubbles vs number of US pulses. This plot excludes large microbubbles that did not respond to US. The number of pulses includes all pulses after the microbubble reached its metastable size. The data are fit to a single exponential, shown as the solid black line; the mean lifetime of the microbubbles is 71.4 pulses.

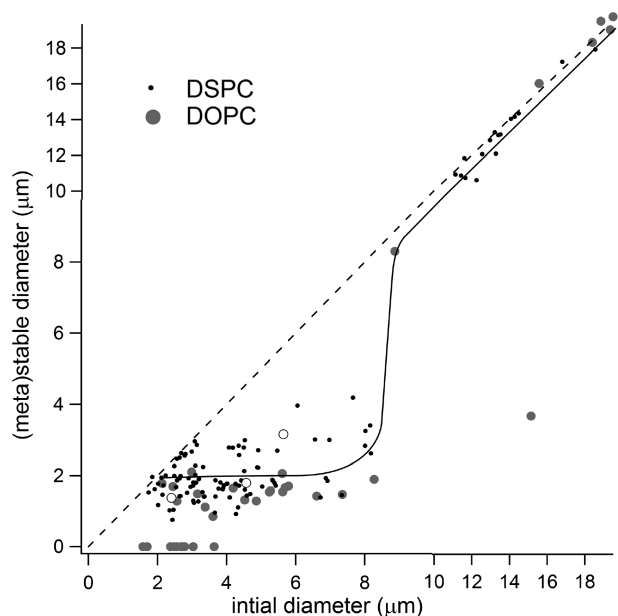


Figure 4. Metastable diameter vs initial diameter for DSPC- and DOPC-coated microbubbles, exposed to a sequence of 300 ultrasound pulses. The dashed line represents no response (final diameter = initial diameter). The solid line is a guide to the eye. DSPC-coated microbubbles smaller than $8.2 \mu\text{m}$ shrank to a stable diameter of $2.1 \pm 0.8 \mu\text{m}$; microbubbles larger than $10.7 \mu\text{m}$ did not change size. DOPC-coated microbubbles smaller than $8.3 \mu\text{m}$ shrank to a metastable diameter of $1.8 \pm 0.7 \mu\text{m}$ and later vanished; microbubbles larger than $8.9 \mu\text{m}$ did not change size. Open circles represent the very few (3) DOPC microbubbles that shrank to a stable size and did not vanish over the time of the experiment.

lipids. Regardless of coat, bubbles with diameters $>9 \mu\text{m}$ were unresponsive. The stable size for DSPC bubbles shows a very slight dependence on initial size, with initially larger bubbles giving slightly larger final sizes. No such dependence is apparent in the metastable sizes for DOPC-coated bubbles.

In the absence of ultrasound, lipid-coated PFB bubbles do not shrink, over many minutes of observation.

3.2. Response of Unshelled Microbubbles to Ultrasound.

Figure 5 shows the final diameter vs initial diameter for unshelled PFB microbubbles. Unshelled microbubbles larger than $\sim 11 \mu\text{m}$ did not change size in response to US. The size threshold for a response is similar to that observed for lipid-coated bubbles, but slightly larger. Unshelled microbubbles smaller than $\sim 11 \mu\text{m}$ were observed to first rapidly fragment, until the core reached an

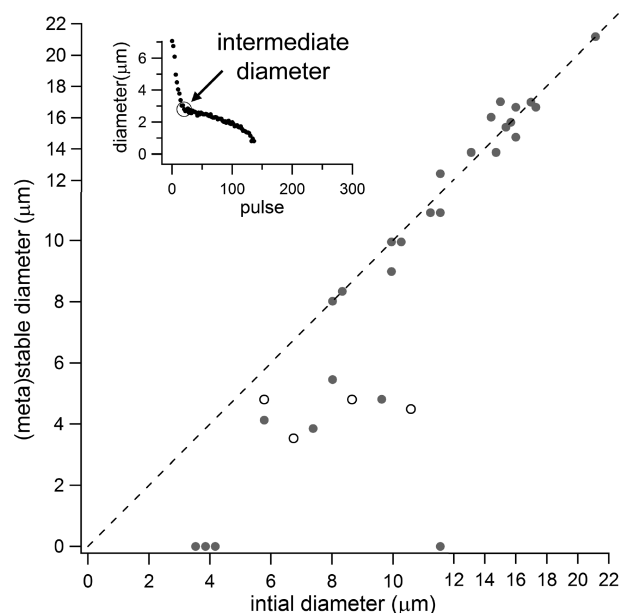


Figure 5. Metastable diameter vs initial diameter for unshelled microbubbles, exposed to a sequence of 300 US pulses. The dashed line represents no response. Microbubbles larger than $\sim 10 \mu\text{m}$ remained the same size; microbubbles smaller than $\sim 10 \mu\text{m}$ vanished entirely. Responding microbubbles fragmented to an intermediate diameter ($\sim 4\text{--}6 \mu\text{m}$), after which they slowly dissolved without further apparent fragmentation until they were no longer visible. Open circles represent the intermediate diameter of microbubbles that exhibited this behavior but did not vanish during the duration of the experiment. These microbubbles continued to shrink after they reached their metastable diameter, by up to 20%, and may have eventually vanished if given more time. Inset: shrinkage of a single unshelled microbubble as a function of number of ultrasound pulses.

intermediate diameter of $\sim 4\text{--}6 \mu\text{m}$. At that point, fragmentation ceased, and they began to shrink at an accelerating rate, without further fragmentation, until they were no longer visible. A typical plot of diameter vs pulse exposure is shown in the inset. Bubbles that did not disappear completely during the experiment (4) were found to follow this same trajectory and thus would likely have vanished had the experiment continued. Three microbubbles with initial diameters smaller than the typical intermediate diameter dissolved away with no apparent fragmentation. Unlike the lipid-coated microbubbles, unshelled microbubbles did not show a metastable size; as seen in the inset, the intermediate diameter is merely an inflection point in the curve of bubble diameter vs pulse number.

In the absence of ultrasound, unshelled PFB-containing bubbles do shrink, as the aqueous buffer is undersaturated with the PFB bubble gas and the Laplace pressure provides an additional, strong driving force for dissolution. However, the time scale for this process is quite slow—on average 152 s, ranging from 24 to 308 s—while the ultrasound experiments reported here are complete within 12 s. More importantly, passive dissolution of uncoated bubbles did not show either a metastable diameter or an inflection point. These results are similar to those of Kwan et al.,²³ who observed passive dissolution of SDS (sodium dodecyl sulfate) coated, SF_6 microbubbles in an air-saturated medium. They saw a brief initial growth phase lasting a few minutes, followed by approximately linear shrinkage to zero, accelerating at the end. Our uncoated PFB bubbles showed a similar approximately linear shrinkage with terminal acceleration; as no special effort was made to observe the bubbles immediately after their formation, any initial growth was not observed.

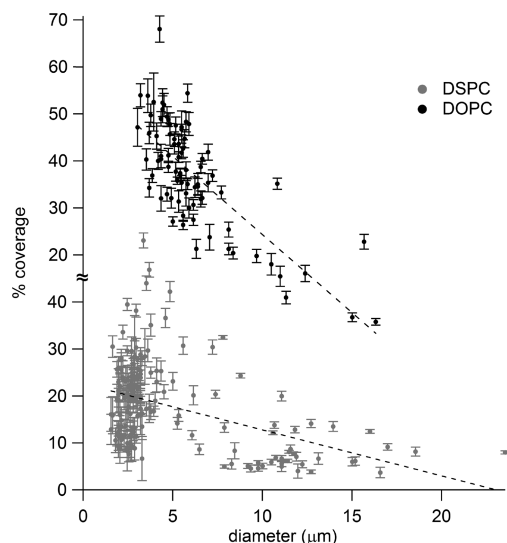


Figure 6. % coverage vs diameter for fluorescent microbubbles. Plots are offset for clarity. The dashed lines represent a linear fit. % coverage is the intensity per area of the microbubbles divided by half the intensity per area of a supported lipid bilayer. There is a small (negative) correlation between microbubble brightness and diameter. The correlation coefficient for DSPC microbubbles is -0.44 and for DOPC microbubbles is -0.75 , each with $P > 99.95\%$. DSPC microbubbles are coated with $18 \pm 9\%$ of a monolayer, and DOPC microbubbles are coated with $37 \pm 12\%$ of a monolayer.

3.3. Fluorescence Measurement of Lipid Shell Density.

To investigate the role of the lipid coat concentration in bubble behavior, coated bubbles were formed using a fluorescent dopant, NBD-DPPE. Microbubbles of two lipid shell compositions (89 mol % DSPC, 10 mol % DSPE-PEG2000, 1 mol % NBD-DPPE and 89 mol % DOPC, 10 mol % DSPE-PEG2000, 1 mol % NBD-DPPE) were imaged using epifluorescence microscopy, and the intensity per unit surface area was calculated for each microbubble.

To estimate absolute (rather than relative) coat concentrations, we compared the bubble fluorescence to the intensity per area for a supported lipid bilayer containing the same probe concentration. Our fluorescent lipid, NBD-DPPE, has the fluorophore attached to the headgroup of the lipid rather than the hydrophobic chains. Given that the fluorophore is in the same PBS environment whether it is in a bilayer or a monolayer, one would expect that the intensity per area of a lipid monolayer would be half that of a bilayer. We therefore express the intensity per area of microbubbles as % coverage, which is the intensity per area of the bubble divided by half of the intensity per area of a lipid bilayer.

Figure 6 shows the coverage vs initial diameter for the two lipid shell compositions. DSPC microbubbles are coated with $\sim 18 \pm 9\%$ of a monolayer, and DOPC microbubbles are coated with $\sim 37 \pm 12\%$ of a monolayer. There is a small correlation between coverage and microbubble diameter, with larger bubbles having somewhat lower coat densities. The correlation coefficient for DSPC microbubbles is -0.44 and for DOPC microbubbles is -0.75 , each with $P > 99.95\%$.

However, these results do not suggest an important role for lipid coat concentration on bubble response for several reasons: (1) DSPC bubbles were most resilient, in that they were never observed to completely dissolve or disappear. Bubbles formed using the same protocol and DSPC concentration had lower coat concentrations than DOPC bubbles, not higher, as would be expected if the initial coat concentration were important to resilience.

Table 1. Model Parameters for the Modified Herring Equation

ρ	liquid density	998 kg/m ³
γ	polytropic gas exponent	1.07
c	speed of sound in liquid	1540 m/s
μ	viscosity of liquid	0.001 Pa s
P_0	hydrostatic pressure	101 kPa
R_0	initial bubble radius	
T_0	initial gas temperature	298 K
Π_0	initial surface pressure	1 mN/m ³⁶
σ_0	initial surface tension	71 mN/m
σ_{bare}	bare interface surface tension	72 mN/m
$\Pi(t)$	surface pressure	
$\sigma(t)$	surface tension	
$T(t)$	gas temperature	
$P_{\text{drive}}(t)$	driving pressure	
$R(t)$	bubble radius	
$\dot{R}(t)$	bubble wall velocity	

(2) Although larger bubbles showed lower coat concentrations and, in addition, no US responsivity, there was no dramatic change in coat concentration at the onset of US responsivity (i.e., for bubbles smaller than $\sim 9 \mu\text{m}$.) Moreover, uncoated bubbles showed a similar size threshold for US response, fragmenting and shrinking only when smaller than $\sim 11 \mu\text{m}$.

3.4. Response Modeling. To better understand microbubble response, we modeled the microbubbles using a modified Herring equation.^{24,25} This is a modification of the Rayleigh–Plesset treatment, in that it includes effects of damping caused by reradiation. The radiation damping enters as a term proportional to the time derivative of the pressure in the liquid adjacent to the bubble \dot{P} :

$$\rho R \ddot{R} + \frac{3}{2} \rho \dot{R}^2 = P + \frac{R}{c} \dot{P} - (P_0 - P_{\text{drive}}(t)) \quad (1)$$

R is the bubble radius; ρ and c are the density and sound speed in the surrounding fluid, respectively. Morgan et al.²⁴ developed this model by using a constant surface tension σ and a (temperature-independent) surface elasticity χ . We chose to include the effects of an adiabatic temperature increase on compression by modeling the surface lipids as a 2D gas with surface pressure Π following $\Pi A/T = \text{constant}$, i.e., a 2D ideal gas law. Then the surface tension is

$$\sigma(t) = \sigma_{\text{bare}} - \Pi(t) \quad (2)$$

The 2D ideal gas law gives

$$\frac{R^2 \Pi}{T} = \frac{R_0^2 \Pi_0}{T_0} \quad (3)$$

where the temperature change can be found from a presumed adiabatic bubble volume change

$$TV^{\gamma-1} = T_0 V_0^{\gamma-1} \quad (4)$$

The surface pressure is then

$$\Pi(t) = \Pi_0 \left(\frac{R_0}{R(t)} \right)^{3\gamma-1} \quad (5)$$

With an initial surface tension of

$$\sigma_0 = \sigma_{\text{bare}} - \Pi_0 \quad (6)$$

(24) Morgan, K. E.; Allen, J. S.; Dayton, P. A.; Chomas, J. E.; Klibanov, A. L.; Ferrara, K. W. *IEEE Trans. Ultrason. Ferroelectr. Freq. Control* **2000**, *47*, 1494–1509.

(25) Vokurka, K. *Acustica* **1986**, *59*, 214–219.

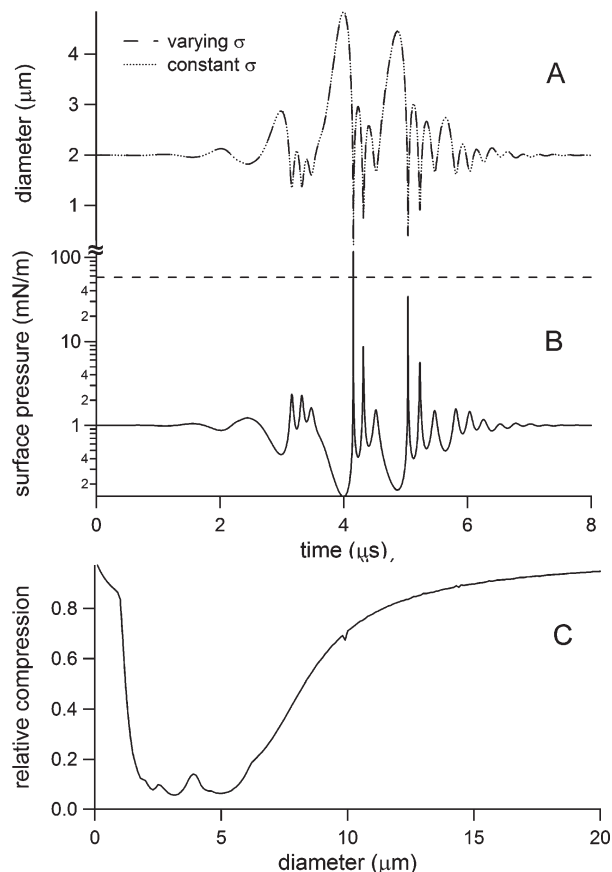


Figure 7. (A) Diameter vs time for both varying (eqs 2 and 5) and constant (72 mN/m) surface tension; they are essentially indistinguishable, showing that surface tension does not play an important role in modifying bubble response. Initial diameter = 2 μm. (B) Surface pressure (log scale) vs time. The dashed line represents the collapse pressure for a DSPC/DSPE-PEG2000 monolayer (48–67 mN/m, the line is shown at 58 mN/m).^{20,36} Surface pressure was calculated from the diameter using eq 5. Initial diameter = 2 μm. (C) Relative compression vs initial diameter, calculated from the modified Herring equation (eq 1). Relative compression is the minimum diameter divided by the initial diameter. The range of responding bubbles is ~1–9 μm. The peaks in response correspond to resonance of the fundamental ultrasound frequency (for 5.3 μm bubbles) and its overtones (3 μm–2.2 MHz and 2.2 μm–3.3 MHz).

This surface tension causes a Laplace pressure difference between the bubble gas and the adjacent liquid. Following exactly the development in the appendix of ref 24, applying this time-dependent pressure term (and ignoring the shell viscosity), one obtains

$$\begin{aligned} \rho R \ddot{R} + \frac{3}{2} \rho \dot{R}^2 = & \left(P_0 + \frac{2\sigma_0}{R_0} \right) \left(\frac{R_0}{R} \right)^{3\gamma} \left(1 - \frac{3\gamma}{c} \dot{R} \right) - \frac{4\mu \dot{R}}{R} \\ & - \frac{2\sigma_{\text{bare}}}{R} \left(1 - \frac{1}{c} \dot{R} \right) + \frac{2\Pi_0}{R} \left(\frac{R_0}{R} \right)^{3\gamma-1} \left(1 - \frac{3\gamma}{c} \dot{R} \right) \\ & - (P_0 - P_{\text{drive}}(t)) \end{aligned} \quad (7)$$

This equation was solved for bubble radius and wall velocity, using Matlab's ordinary differential equation solver, with initial conditions $R = R_0$ and $\dot{R} = 0$. The driving pressure for the modeling was taken from a direct measurement of the experimental ultrasound pulse, described in the Materials and Methods section.

In fact, whether the surface tension was held constant at 72 dyn/cm or varied according to the 2D ideal gas model made little difference in the results. Figure 7 shows the predicted bubble

response using a three-cycle pressure wave input taken from the measured ultrasound pulse. The effect of surface tension/surface pressure on bubble response was negligible, even when the surface tension was allowed to become negative (surface pressure greater than 72 dyn/cm) during bubble compression (Figure 7B). Although the exact amplitude of the pressure wave is somewhat uncertain (owing to angle variations in transmission through the cuvette walls and reflections from the upper wall), it is likely that the positive overpressures were sufficient to reduce the bubble surface area below that required to accommodate the surface lipids (Figure 7B), *assuming isotropic compression*. Of course, the modified Herring equation (and the Rayleigh–Plesset equation) both *assume* isotropic bubbles.

The modeling studies may shed some light on the responsive range of bubble diameters (Figure 7C). The modified Herring equation predicts large bubble responses for diameters from ca. 1 to 9 μm. The large responses appear to be due in part to a consonance of the resonant frequencies of bubbles with either the fundamental ultrasound frequency (for 5.3 μm bubbles) or its overtones (3 μm–2.2 MHz and 2.2 μm–3.3 MHz), where these theoretical resonant frequencies were determined by measuring peak-to-peak of the ring-down of the calculated bubble responses. The exact shape of the response curve is complicated, owing to the strong nonlinearities.

4. Discussion

There are three central issues presented by these results. (1) Why do bubbles shrink? (2) Why do (coated) bubbles stop shrinking? Lastly, (3) why do bubbles coated with the unsaturated lipid DOPC eventually dissolve, while bubbles with saturated DSPC coats persist indefinitely?

4.1. Why Do Bubbles Shrink? The shrinking of larger bubbles, reported here and observed by others as well,^{9,11,12,18,20,23} is likely caused simply by the loss of the perfluorobutane gas through dissolution into the aqueous solution. The evidence for this is that uncoated PFB bubbles do shrink over time, in the absence of ultrasound. The rapid expansion and contraction of the bubbles caused by the ultrasonic pressure wave apparently enhances the rate of gas dissolution, as uncoated bubbles take many minutes to shrink in the absence of ultrasound and coated bubbles are essentially stable. The enhancement in the rate of gas transport may be caused by the very large increase in the pressure and chemical potential of the gas during compression; the convection of fluid surrounding the bubble during the oscillation may also contribute.

Larger microbubbles showed no response to the ultrasound. It has been observed previously²⁶ that for microbubbles with thick shell consisting of a lipid monolayer and an additional layer of oil a longer US pulse is required to make the microbubble fragment, compared with a lipid-monolayer-coated microbubble. This suggests that a microbubble with a thicker shell is more resilient. To ascertain whether bubble coat density might play a role in the unresponsiveness of the larger bubbles, we measured the fluorescence of lipid-coated microbubbles, doped with 1 mol % fluorescent lipids. We found that fluorescence intensity per unit surface area actually *decreased* slightly for larger bubbles (Figure 6). This result, and the fact that large, unshelled bubbles also show no US response, indicates that the presence or absence of an US response is not caused by the coat. Rather, large bubbles appear to be unresponsive because their fundamental resonance frequencies

(26) May, D. J.; Allen, J. S.; Ferrara, K. W. *IEEE Trans. Ultrason. Ferroelectr. Freq. Control* **2002**, *49*, 1400–1410.

are well below the frequency of the US pulse, as we found with mathematical modeling using the modified Herring equation.

In some cases, US-induced bubble “shrinkage” can actually result from fragmentation. This mechanism was observed with unshelled microbubbles larger than 4–6 μm in diameter. Lipid-coated microbubbles did not show visible fragmentation, but we cannot rule out fragmentation of submicrometer bubbles as a contributing mechanism for their shrinkage. Borden et al.¹⁸ saw lipid-coated microbubbles visibly fragment under US, but the US pressure was much higher than ours (800 kPa); they did not see fragmentation for lower US pressure (400 kPa). Fragmentation may be a consequence of parametric excitation of bubble surface modes²⁷ or from intrinsic asymmetry (owing to the presence of a nearby wall, for example). It obviously cannot emerge from the spherically symmetric modified Herring model, and other physical factors will have to be incorporated to develop a fuller understanding of this process.

Chomas et al.²¹ found empirically the phase of the ultrasound pulse can affect fragmentation of a commercial contrast agent (MP1950), which has a PFB gas core and a phospholipid shell. Pulses with rarefaction prior to compression (a phase of 180°) caused fragmentation, while the opposite phase (0°) was ineffective, for small bubbles responding in phase with the pulse. As bubble size is decreased, the phase of the response to an ultrasonic pulse will vary from 180° (out of phase with the US pulse) for a very large diameter bubble (driven well above its resonant frequency) to 0° (in phase with the US pulse) for a very small diameter bubble (driven well below its resonant frequency).^{24,28,29} The crossover, at resonance, should occur at 5.3 μm for the 1.1 MHz ultrasound used here. The fact that smaller unshelled microbubbles do not visibly fragment may thus be a consequence of the phase of their response.

4.2. Why Do Bubbles Stop Shrinking? Microbubbles with lipid coats typically reached a stable or metastable size of $\sim 2 \mu\text{m}$ in diameter (although some DOPC-coated bubbles showed prompt dissolution.) A stable size for lipid-coated microbubbles has been seen before. Borden et al.¹⁸ observed dissolution of PFB microbubbles when exposed to short pulses of ultrasound (2.25 MHz, 400 kPa PNP, 0.5 Hz repetition rate). They used microbubbles with several different lipid shells (saturated lipid (DMPC, DSPC, or DBPC), with 10 mol % emulsifier (DSPE-PEG2000, DMPE-PEG2000, or PEG 40 stearate)). They found that all of their microbubbles shrank to a stable diameter of about 1–3 μm and remained at that size indefinitely. Guidi et al.³⁰ found that saturated phospholipid-coated perfluoropropane bubbles shrink to a stable size of about 1.5 μm when exposed to pulses of ultrasound (2–4 MHz, 49–62 kPa, 250 Hz repetition rate).

The reason for stability (or for the associated stable size) is not known. Rectified diffusion has been suggested to play a role;¹⁸ however, the importance of the lipid shell argues against this. (Uncoated microbubbles, exposed to the same US pulses, do not show a stable size.) Our results, and those of the other researchers mentioned above, are all the more remarkable in that modeling shows that the minimum bubble size (at peak US overpressure) is too small to accommodate the lipid coat on the bubble surface. The modeling results are largely insensitive to the specific surface tension model used—it seems certain that the lipid coat has

insufficient compressive strength to *prevent* the bubble collapse. Since uncoated bubbles are unstable and dissolve spontaneously, the stability of bubbles coated with saturated lipids implies that the lipids are able to recoat the bubble on expansion (or after the brief three-cycle pulse.)

Katihar et al.³¹ modeled bubble dissolution via gas transport from the bubble to the surrounding medium in the absence of ultrasound. They found that the bubble would shrink to a stable size if the medium is saturated with air (even if the bubble gas is not air) and if the shell elasticity can equal the surface tension. This may help explain results like Feshitan et al.¹⁰ and Kwan et al.²³ (a stable size without ultrasound), but it is not clear that it is relevant to the stable size of bubbles in ultrasound. In particular, the equating of the elasticity with the surface tension is equivalent to a net zero surface tension, and lipid monolayers collapse in compression well before zero surface tension is reached. In addition, Katihar et al. assume the bubble wall velocity is slow compared with the rate of gas transport and thus neglect convection in the fluid. In our modeling of the modified Herring equation, we found that the maximum bubble wall velocity is 330 m/s for a 2 μm diameter bubble, which is clearly much faster than the rate of gas transport.

4.3. Why Does the Unsaturated Lipid DOPC Provide Only a Metastable Size? While bubbles coated with DSPC/10 mol % PEG-lipid were stable throughout the experiment, bubbles coated with DOPC/PEG-lipid were only metastable.

It is possible that the saturated and unsaturated lipids behave very differently during the extreme compression. For example, the saturated lipids, which should form a solid monolayer, may “pancake” during compression, while the unsaturated fluid phase lipid monolayer may buckle and form looser folds, which can lead to the formation of “semivesicles” and other intermediary structures.³² We note also that DSPC has been observed to phase separate from the PEG-lipid used for steric stabilization of these bubbles;^{11,33,34} such phase separation could possibly lead to mechanically weaker lines along which bending fracture during compression could occur.

A number of studies have indicated that microbubbles (in the absence of ultrasound) can shed fluid phase lipids more readily than solid phase, saturated lipids. Bubbles coated with short chain lipids appear (by bright-field microscopy) to be smooth and spherical during dissolution, while bubbles coated with long chain lipids become wrinkled and nonspherical, as a result of monolayer stresses from crowding.^{11,20} Air-filled microbubbles made from seawater (a majority of the coat was short chain and unsaturated fatty acids and lipids) also appeared smooth throughout dissolution.³⁵ Dissolution of fluorescent microbubbles in a degassed medium found that bubbles coated with short chain lipids either did not visibly shed any shell material as it shrank (presumably the shell was shed continuously as micelles) or formed small ($\sim 1 \mu\text{m}$) vesicles that were seen being shed continuously from the shrinking bubble.^{11,12} Fluorescent microbubbles coated with long chain lipids generally formed large aggregates or tubelike structures that remained attached to the bubble as it shrank.^{11,12} All of this indicates that a bubble coated with short chain or unsaturated lipids (such as DOPC) can more readily shed its shell material in

(27) Versluis, M.; van der Meer, S. M.; Lohse, D.; Palanchon, P.; Goertz, D.; Chin, C. T.; de Jong, N. Proceedings of the 50th Ultrasonics Symposium, IEEE, Montreal, 2004.

(28) Sun, Y.; Kruse, D. E.; Dayton, P. A.; Ferrara, K. W. *IEEE Trans. Ultrason. Ferroelectr. Freq. Control* **2005**, *52*, 1981–1991.

(29) Neppiras, E. A. *Phys. Rep.* **1980**, *61*, 159–251.

(30) Guidi, F.; Vos, H. J.; Mori, R.; de Jong, N.; Tortoli, P. *IEEE Trans. Ultrason. Ferroelectr. Freq. Control* **2010**, *57*, 193–202.

(31) Katihar, A.; Sarkar, K.; Jain, P. *J. Colloid Interface Sci.* **2009**, *336*, 519–525.

(32) Baoukina, S.; Monticelli, L.; Risselada, H. J.; Marrink, S. J.; Tieleman, D. P. *Proc. Natl. Acad. Sci. U.S.A.* **2008**, *105*, 10803–10808.

(33) Borden, M. A.; Pu, G.; Runner, G. J.; Longo, M. L. *Colloids Surf., B* **2004**, *35*, 209–223.

(34) Borden, M. A.; Martinez, G. V.; Ricker, J.; Tsvetkova, N.; Longo, M.; Gillies, R. J.; Dayton, P. A.; Ferrara, K. W. *Langmuir* **2006**, *22*, 4291–4297.

(35) Lozano, M. M.; Talu, E.; Longo, M. L. *J. Geophys. Res., [Oceans]* **2007**, *112*.

(36) Chou, T. H.; Chu, I. M. *Colloids Surf., B* **2003**, *27*, 333–344.

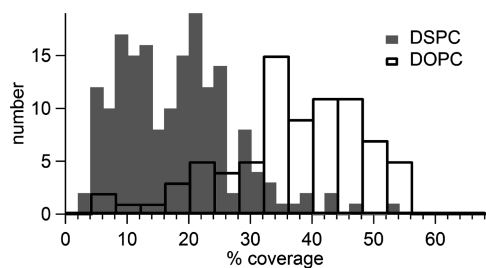


Figure 8. Distributions of initial lipid coat concentrations for DOPC- and DSPC-coated microbubbles.

the form of small vesicles or micelles when it shrinks, while a bubble coated with long chain saturated lipids (such as DSPC) will not easily part with its shell material when it shrinks.

Somewhat remarkably, the lifetime distribution of DOPC-coated bubbles was exponential (Figure 3). A priori, the lifetime distribution could be a consequence of the variation in lipid shell densities. In the simplest model, a certain fraction of the remaining coat would be shed in each pulse; when the coat goes below a critical concentration, dissolution follows rapidly. In this “fractional coat-shedding model”, a bubble survives exactly n pulses if it begins with a coat concentration $C_0 = C_{\text{crit}}e^{n/\eta}$, where η is the number of pulses that reduce the coat density by a factor of e and C_{crit} is the critical concentration for onset of dissolution. The fraction of bubbles that survive exactly n pulses is then given by

$$F(n) = \frac{C_{\text{crit}}}{\eta} e^{n/\eta} F(C_0)$$

where $F(C_0)$ is the fraction of bubbles that have an initial coat concentration between C_0 and $C_0 + dC$. For $F(n)$ to be a simple exponential decay (Figure 3), $F(C_0)$ would have vary as an inverse power (> 1) of C_0 ; such an unusual distribution for coat concentrations is not observed (Figure 8). Thus, this simple deterministic model cannot fit our observed results. Rather, the exponential lifetime distribution suggests that there is a single, “catastrophic”, and probabilistic shedding event, subsequent to which the bubble quickly dissolves entirely.

5. Summary and Conclusions

The ability of moderately intense, but biomedically relevant 1.1 MHz ultrasound to cause shrinkage of lipid-coated microbubbles has been well established. We have reconfirmed this result but also found significant differences in bubble behavior that depend on both initial size and the composition of the lipid coat. Large ($> \text{ca. } 10 \mu\text{m}$ diameter) bubbles were unresponsive, regardless of the coat (or even absence of any coat), while smaller bubbles ($2\text{--}10 \mu\text{m}$ diameter) showed an initial rapid decrease in size to a small stable or metastable/intermediate diameter. With uncoated bubbles, the initial reduction in size appeared to be caused by *fragmentation*, while no fragments of coated bubbles were seen. The intermediate diameter had no persistence for the uncoated bubbles but merely represented a (nearly) discontinuous change in the *rate* of shrinkage; moreover, no fragments were observed during this second phase of uncoated bubble dissolution. With an unsaturated (DOPC) coat, the intermediate state was truly metastable, often persisting with no observable change for more than 100 ultrasound pulses. Finally, with a saturated (DSPC) coat, the small diameter bubbles persisted indefinitely, as has been previously reported.

The different responses of bubbles with different coats must reflect different behavior of the coat molecules under extreme (2D) compression and expansion. The complete disappearance of a coated bubble likely requires the “shedding” of any coat, in the sense that the coat molecules can no longer be associated with a gas–liquid interface. The stability of $2 \mu\text{m}$ diameter DSPC-coated microbubbles (compared with uncoated bubbles) implies that the coat, or at least part of it, remains associated with the bubble.

In this study, we also used a numerical solution of the modified Herring equation (a variant of the Rayleigh–Plesset equation) for bubble motion in order to determine whether bubble responses correlated with predicted amplitudes of bubble oscillations, wall velocities, etc. Qualitatively, the maximal responses for bubbles between 2 and $10 \mu\text{m}$ correlated well with the resonance of bubbles of this size range with the applied 1.1 MHz ultrasound frequency. However, the modeling results also suggest that bubble surface area compression, even for the $2 \mu\text{m}$ bubbles, is far in excess of maximum lipid monolayer compression, assuming an isotropic compression. Thus, during maximum compression, the lipid coat can no longer be maintained as an interfacial monolayer and must form other structures that can rapidly recoat the bubbles during the expansion.

The differences in the behavior of DSPC- and DOPC-coated bubbles could possibly arise from several different factors. First, it is quite likely that bubbles cannot remain isotropic at maximal compression, since, as noted above, the lipid coat cannot fit on the available surface. Thus, the modified Herring equation modeling shows that some kind of failure of the lipid shell must occur. The details of this failure (e.g., crumpling vs pancaking) may affect the ability of the lipid shell to recoat during the bubble expansion. It is noteworthy that these saturated DSPC/DSPC-PEG coats have been reported to laterally phase separate.^{11,33,34} Lateral phase separation could readily produce lines of weakness that affect the shell failure. Acyl chain melting cannot be ruled out, either. Even though the modeling predicts temperatures far in excess of the DSPC melting temperature ($100 \text{ }^\circ\text{C}$), if the shell failure occurs before the bubble reaches the smallest sizes, the model estimate of the adiabatic temperature increase could be far in excess of the actual temperature reached. Thus, either lateral phase separation, or chain melting phase behavior, could be responsible for the remarkable difference in DOPC vs DSPC coated bubble behavior.

This work, and prior work of other researchers cited here, shows the importance of the initial microbubble diameter in affecting the responsivity of microbubbles to ultrasound. This knowledge is especially useful for biomedical applications of microbubbles; with the recent development of new techniques for the preparation of bubbles with highly monodisperse size distributions,^{13,14,16,17} tailoring the size of an entire population of bubbles to maximize response now becomes feasible. We have also identified an important role for microbubble shell composition in the ultrasound response, confirming the presence of a stable size for bubbles with saturated lipid coats, and demonstrating that bubbles with unsaturated coats can be completely disrupted. These distinctive behaviors should prove useful in designing US-triggered drug carriers.

Acknowledgment. This work was supported by the “Integrating Nanoscience with Cell Biology and Neuroscience” IGERT program, NSF Grant 0549500.